This is the accepted manuscript made available via CHORUS. The article has been published as:

Role of photonic angular momentum in all-optical magnetic switching

Muhammad Waleed Khalid, Ali Akbar, Jeongho Ha, Mohammed Salah El Hadri, Alexander V. Sergienko, Eric E. Fullerton, and Abdoulaye Ndao

Phys. Rev. B **109**, L140403 — Published 9 April 2024

DOI: 10.1103/PhysRevB.109.L140403

Role of photonic angular momentum on all-optical magnetic switching

Muhammad Waleed Khalid,[1,*] Ali Akbar,[2] Jeongho Ha,[1,*] Mohammed Salah El Hadri,[3] Alexander V. Sergienko,[2] Eric E. Fullerton,[1] and Abdoulaye Ndao[1,†]

[1] *Department of Electrical and Computer Engineering, University of California-San Diego, La Jolla, CA, USA.*

[2] *Photonics Center, Boston University, 8 St. Mary's Street, Boston, MA 02215, USA.*

[3] *Western Digital Corporation, 5601 Great Oaks Parkway, San Jose, 95119, CA USA*

(Dated: March 26, 2024)

Abstract

We report on the role of light's angular momentum in magnetic all-optical switching (AOS), which entails magnetization reversal resulting from ultrafast laser pulses applied to a magnetic structure. The magnetic system is comprised of a ferromagnetic thin film of Co/Pt, excited by femtosecond vortex beams of light carrying spin, orbital angular momentum, or a superposition of both. We find that AOS is predominantly driven by the spin angular momentum of light. The experimental findings suggest that the magnitude of topological charge and handedness of the orbital angular momentum of light do not play a significant role. These results improve our understanding of the basic interactions between magnetism and light, paving the way for further investigation and the creation of all-optical magnetic switching technologies.

I. INTRODUCTION

The field of ultrafast laser manipulation of magnetization has witnessed significant advancements in the past twenty years across different engineered materials [1, 2]. In the context of magnetic materials, it can be observed that a laser pulse serves as the most rapid stimulus to the system because it interacts with a magnet at a significantly higher speed compared to the fundamental interactions occurring between the electrons, magnetic lattices, and spins. Laser pulses exhibit the characteristic of serving as carriers of magnetic fields, resulting in the instantaneous magnetization of materials in a predictable orientation. For some systems utilizing of femtosecond (fs) laser pulses, can further deterministically control the final state of magnetization commonly referred to as all-optical switching (AOS) [3].

Past studies of the interaction between light and magnetic materials have primarily focused on the polarization of light, specifically, how circularly polarized light carrying spin angular momentum (SAM), $\mathbf{S}$ [4] interacts differently with magnetic substances [5–9]. The deterministic magnetization switching using circularly polarized laser pulses is known as helicity-dependent AOS in which the helicity of the input circular polarization of the electromagnetic wave determines the final state of the magnetization [5, 10]. Despite AOS

* Also at Photonics Center, Boston University, 8 St. Mary's Street, Boston, MA 02215, USA.

† a1ndao@ucsd.edu; Also at Photonics Center, Boston University, 8 St. Mary's Street, Boston, MA 02215, USA.

being successfully demonstrated in both ferri- and ferro-magnetic thin films [2, 7, 11, 12], the mechanism of this process is still a topic of debate in the scientific community. Several models have been presented to explain AOS. These include local effective fields created by the circularly polarized light via the inverse Faraday effect (IFE) [13] as a source for magnetic switching. In contrast, the transfer of SAM from light to the magnetic material [14, 15] and magnetic circular dichroism (MCD) [11] have also been modeled to explain AOS. However, recent experiments have pointed to the fact that MCD is a contributing or even dominant mechanism of AOS in ferromagnetic materials. In MCD, one magnetic domain orientation favors the absorption of light with a particular helicity over the other, and temperature gradient across domain walls [8] or difference of temperature of individual grains [16], induced by the differential absorption, switches the magnetization. It was experimentally shown that switching is possible only with multiple-pulse excitation described as a two-step process [5, 17, 18]. The first step is independent of the SAM of the input pulses as these pulses demagnetize the sample, bringing it to a multidomain state. The second step is dependent on the SAM as these pulses grow magnetic domain in a preferred orientation, which is determined by the helicity of light.

However, the effect of optical beams with orbital angular momentum (OAM), $\mathbf{L}$ on AOS is unknown. This makes our understanding incomplete and raises important questions: can the OAM of light trigger electronic transitions to change the net magnetization of the system? These transitions may establish photon absorption and emission patterns based on photonic OAM handedness and magnitude. The coupling between optical vortex beams, which carry OAM, and magnetic media has been demonstrated through spectroscopic analysis of the ferrimagnetic material dysprosium iron garnet at THz frequency [19]. The study found that magnetism can be probed with a vortex beam through channels of vortex dichroism i.e., the differential rate of absorption for different handedness of the vortex beam. The study also suggested that magnetic excitations of garnet depend on both the handedness of the vortex beam and the direction of the beam propagation with respect to the sample magnetization. Recently, it has been shown that the IFE in metals, in addition to SAM of light, can be induced by the OAM of light as well [20]. Notably, the relative contributions of SAM and OAM to the IFE have been quantified in a thin gold film irradiated by beams carrying SAM and/or OAM. This understanding of OAM's function in regulating the IFE and the ensuing optomagnetics field adds a new dimension to the study of all-optical magnetization.

Nonetheless, in Pt/Co thin films, simulations show that it can only be switched magnetically with an optically induced magnetic field of tens of Tesla [21]. This revelation eliminates the IFE connection to the light's OAM as the main mechanism for magnetic switching. Thus, we predict vortex dichroism as the mechanism for this phenomenon. Our research builds on the novel work in [17], which investigates all-optical control of ferromagnetic thin films and nanostructures. Recent research on helicity-dependent all-optical switching in Co/Pt ferromagnetic multilayers has shown complicated magnetization dynamics and the possibility of material-specific AOS processes [5].

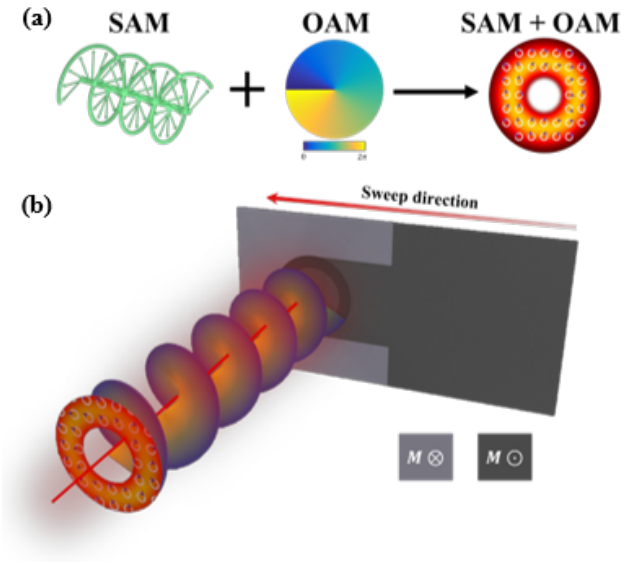


FIG. 1. (a) Beam carrying SAM and OAM. (b) All-optical magnetic switching using beams carrying SAM and OAM.

II. EXPERIMENTAL SETUP FOR AOS

To examine the impact of photonic angular momentum on the process of all-optical magnetization switching in ferromagnetic thin films, our study employs VBs that possess solely OAM **L** as well as those that possess both SAM and OAM **S** + **L** (Fig. 1). We experimentally explore the effect of OAM on the AOS using the experimental setup shown in Fig. 2. It is composed of two main systems: illumination and imaging. For illumination, we illuminate the sample with an optical pulse train. The laser, with a Gaussian spatial profile, passes through the polarizer *P1*, oriented parallel to the optical table, and then

passes through the 50/50 non-polarizing beam-splitter (*NPBS1*). The transmitted output from the *NPBS1* hits the beam dump and the reflected output goes to the spatial light modulator (SLM). Depending on the encoded hologram, the SLM modulates the phase of the incident beam. Ideally, the generation of OAM beam is performed by the following phase hologram encoded on the SLM:

$$\Phi_{SLM} = mod[L\phi, 2\pi] \tag{1}$$

where *mod* is the modulus function and **L** is the topological charge of the desired beam and can, theoretically, take values from 1 to infinity [22].

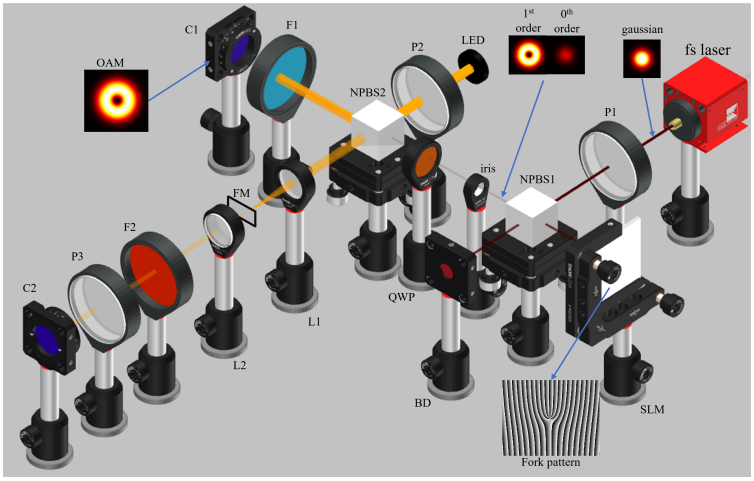


FIG. 2. Experimental setup for observing the effect of OAM and SAM on AOS. *P1-P3*: polarizers, *NPBS1-NPBS2*: non-polarizing beamspiltter, *SLM*: spatial light modulator, *L1-L2*: lenses, BD: beam dump, *C1-C2*: camera, *QWP*: quarter-waveplate, *FM*: ferromagnetic thin film. *F1* and *F2*: 635nm and 800nm notch filters respectively.

The order of **L** is often limited by the experimental factors but most importantly by the resolution of the SLM. Due to the discrete nature of the SLM screen, consisting of liquid crystal cells, it is not 100% efficient in modulating the phase. Any unconverted beam accompanies the modulated beam and interferes with it when incident on a screen. Often, producing an OAM beam with a spiral phase pattern results in the superposition of an unconverted Gaussian and a modulated OAM beam. To resolve this issue, we introduce a spatial carrier frequency: a blazed grating. For experimental generation of the vortex beams, we encode the SLM phase by

$$\Phi_{SLM} = mod[\mathbf{L} + 2\pi(G_{xx} + G_{yy}), 2\pi] \tag{2}$$

where ϕ is the azimuthal coordinate, G_x and G_y are the grating frequencies for the blazed grating along the x and y directions, respectively. The blazed grating in conjunction with a spiral phase pattern results in a fork-like pattern, as shown in the first row of Fig. 3. The magnitude of topological charge, **L**, can be determined by counting the difference between fork tines on top and bottom. Conventionally, if **L** is positive, the fork points up and if **L** is negative, the fork points downwards. We then use an iris to let the first diffraction order, VB carrying OAM, pass into the system and block the unconverted Gaussian beam. The horizontally polarized beam passes through the *QWP* to convert it into circularly polarized light which is then incident on the *NPBS2*. One arm of this beam splitter goes to camera *C1*, and the other arm is incident on ferromagnetic film through a lens *L1* with a small $NA = 0.30$. A lens with a small NA is necessary for our study as it keeps us in paraxial regime to observe the effects of OAM and SAM separately (see Supplementary II).

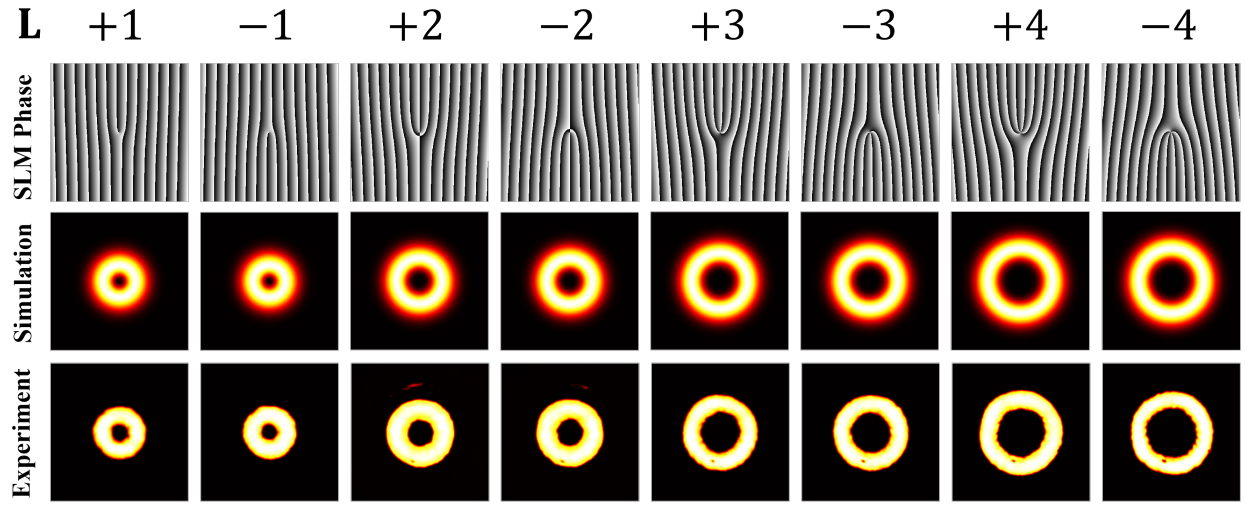


FIG. 3. First row: SLM holographic fork phase pattern for generating OAM beams, with the topological charge, **L**, written on the top. Second and third row: theoretical and experimental intensity profiles for the corresponding OAM beams.

We then use a 800 nm notch filter *F2* to block this beam from hitting the camera *C2*. By using an SLM, we then start generating the OAM-carrying VB to use them for AOS. The first row of Fig. 3 shows the holographic phase pattern of the SLM with a phase profile given by Eq. 1. In the simulation, we choose the Laguerre-Gaussian (LG) mode as the OAM-carrying VB, which is shown in the second row of Fig. 3. Third row only shows the first order of the diffracted VB from the SLM. The intensity of LG beam can be obtained from

their complex amplitude, which increases with the magnitude of L and not its sign. We can observe good agreement between the simulations and the experimentally generated OAM-carrying VB, with similar intensity distributions for a value of L. For imaging, the response of the magnetic film to the circularly polarized OAM beams is then observed through a Faraday microscope. A spatially uniform, linearly polarized, quasi-collimated white light source (Thorlabs SLS201L), with a 650±40 nm bandpass filter, is incident on the sample and is collected by a lens for observing AOS in the ferromagnetic film. LED's initial polarization rotates due to the Faraday effect depending on the sample's magnetization ($\boldsymbol{M}\odot$ or $\boldsymbol{M}\otimes$). The clockwise or anti-clockwise rotation of LED polarization and the analyzer gives the contrast to identify the two distinct magnetic orientations. A monochromatic CMOS camera enables us to capture the impact of these different magnetization orientations on the sample. A 50/50 non-polarizing beam-splitter (*NPBS2*) is used to overlap the imaging source and the laser beam, allowing for direct imaging of magnetization after the laser excitation. The reflective arm of the LED is blocked from reaching the camera *C1* using a notch filter, *F1*.

III. RESULTS

To experimentally explore AOS in ferromagnetic materials, we use perpendicularly magnetized $[\text{Pt}(0.7\text{ nm})/\text{Co}(0.6\text{ nm})]_N$ multilayers where N is the number of [Pt/Co] bilayers in the thin film, which is $N = 1$ in our experiments. The perpendicularly magnetized ferromagnetic thin films were grown on glass substrates by a DC magnetron sputtering system with a base pressure of 3×10^{-8} Torr. These thin films are composed of glass substrate/Ta(3nm)/Pt(3nm)/$[\text{Pt}(0.7\text{nm})/\text{Co}(0.6\text{nm})]_1$/Pt(3.7 nm). The film deposition was performed at room temperature and in an Argon (Ar) gas atmosphere. The Ar pressure during the deposition was 2.7 mTorr.

Before we investigate the effect of OAM on AOS, we start the experiment with $\mathbf{L} = 0$, to show the role of SAM in AOS in ferromagnetic thin films as part of a control experiment. After the initial alignment of the magnetic domains using a permanent magnet, we illuminate the sample with an optical pulse train from Ti:Sapphire laser amplifier system (Solstice from Spectra-Physics) with a central wavelength $\lambda_o = 800$ nm with a 35 fs pulse duration at the source, and 1 kHz repetition rate. For a fair comparison, in both the initial magnetizations $\boldsymbol{M}\odot$ or $\boldsymbol{M}\otimes$, the fs pulses incident on the ferromagnetic material had the same fluence

for all three values of **S**. The dark or white contrast in Fig. 4 corresponds to a reversal of the initial magnetization to the other direction. Using a motorized linear translation stage, the ferromagnetic sample is swept at a speed $10\mu\text{m}/s$ for $50-60\mu\text{m}$ while the thin film is exposed to fs pulses. The response of the magnetic film to the optical pulses, with different initial magnetization states and values of **S**, is then observed through a Faraday microscope.

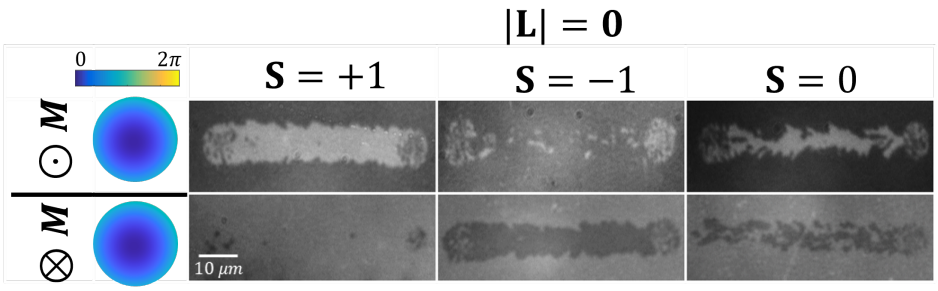


FIG. 4. The initial magnetization of the ferromagnetic sample is either $\boldsymbol{M}\odot$ or $\boldsymbol{M}\otimes$. For each initial magnetization state, we sweep $\mathbf{S}=+1,-1$ and 0 for $|\mathbf{L}|=0$

The first row in Fig. 4 corresponds to the initial magnetization of $\boldsymbol{M}\odot$. The value of **S** will determine the orientation of the magnetization reversal. When the initial magnetization is $\boldsymbol{M}\odot$, the $\mathbf{S}=+1$ optical pulses reverse the magnetization, as shown by the white contrast. Meanwhile, the $\mathbf{S}=-1$ pulses do not switch the initial magnetization. When pulses with $\mathbf{S}=0$ are incident on the ferromagnetic material, the observed phenomenon is the average of the responses to optical pulses with $\mathbf{S}=+1$ and $\mathbf{S}=-1$. It is worth noting that when the initial magnetization is $\boldsymbol{M}\otimes$, we observe the opposite, i.e., $\mathbf{S}=-1$ optical pulses reverse the magnetization, as shown by the dark contrast, but $\mathbf{S}=+1$ pulses are unable to switch the initial magnetization. For $\boldsymbol{M}\otimes$, the $\mathbf{S}=0$ incident on ferromagnetic material exhibits an average effect of $\mathbf{S}=+1$ and $\mathbf{S}=-1$ optical pulses.

Similarly to its counterpart, SAM, the initial guess was to drive AOS with OAM, which might depend on the handedness of OAM, i.e., vortex dichroism or the magnitude of topological charge, **L**. To investigate our hypothesis, we observe AOS using topological charges **L** ±1, ±2, ±3 and ±4. For each topological charge, **L**, we set the value of **S** to be $+1$, -1, or 0. Like $\mathbf{L}=0$, we start with the alignment of the magnetic domain to point either into the plane or out of the plane of the magnetic thin film. For a single value of $|\mathbf{L}|$, we illuminate the sample with $\mathbf{S}=+1,-1$ or 0 and $\boldsymbol{M}\odot$ or $\boldsymbol{M}\otimes$, which makes a total of twelve sweeps for

each. What we observe here is similar to the $|\mathbf{L}| = 0$ case. We see the magnetization reversal only depends on the handedness of SAM and circular dichroism, while it is indifferent to the OAM handedness and vortex dichroism. Even increasing the magnitude of the $\mathbf{L}$ from 1 to 4 does not have any impact on the symmetry breaking. The only notable difference was the variance in the magnetization reversal areas. This can be explained by the larger beam size of the VBs, which is attributed to a larger $\mathbf{L}$; as the value of $\mathbf{L}$ increases, the size of the VB increases, as seen in Fig. 5. To compensate for this reducing intensity, we increase the average power of the input pulses. This ensures that our operations are above the AOS-required threshold fluence and below the potential damage level. Due to the varying size of intensity profiles, we use average power as the parameter to optimize AOS for each $|\mathbf{L}|$. For a fair comparison, the average power of the input laser and its corresponding laser spot size incident on the ferromagnetic film is fixed for each $|\mathbf{L}|$. The average power needed for topological charge $|\mathbf{L}| = 1, 2, 3$ and 4 are 40μW, 50μW, 62μW and 72μW respectively.

To ensure this process is indeed AOS, which is reversible and then repeatable, we realign the magnetization direction using a permanent magnet and then repeat the experiments on the same area of the ferromagnetic sample. According to our findings, the symmetry breaking in the AOS process depends only on the handedness of the SAM and circular dichroism, with the handedness of the OAM and vortex dichroism being unimportant. This is comparable to the case of $\mathbf{L} = 0$. Interestingly, the symmetry breaking was unaffected by increasing the magnitude of $\mathbf{L}$ from 1 to 4. The variance in the areas of magnetization reversal, which can be related to the increased beam size of the VBs with increasing $\mathbf{L}$. The experimental results are similar to a previous study that demonstrates the optical activity by vortex beams for chiral molecules [23, 24]. The study found that there was no influence of the handedness of OAM of light on the optical activity of chiral molecules and exhibit no differential rate of absorption. In paraxial approximation, it is understood in terms that the whole sample is subjected to the vortex beam, hence the corresponding vortex component of absorption rate averages to zero [25]. In contrast to previous studies showing AOS, we have investigated the interplay between OAM and SAM, and its effect on AOS.

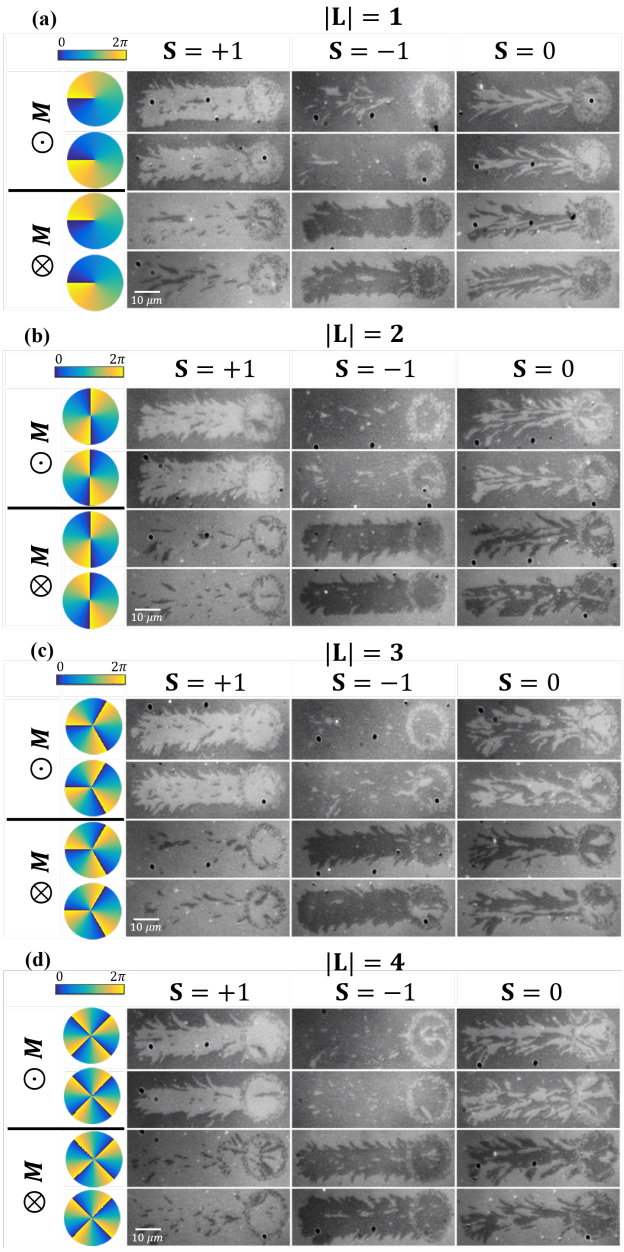


FIG. 5. The initial magnetization of the ferromagnetic sample is either $\boldsymbol{M}\otimes$ or $\boldsymbol{M}\odot$. For each initial magnetization state, we switch between either $+\mathbf{S}$ and $-\mathbf{S}$ and sweep $\mathbf{S} = +1, -1$ and 0. (a)-(d): L takes the values $\pm 1, \pm 2, \pm 3$ and ± 4 respectively for each value of $\mathbf{L}$

IV. CONCLUSION

We have explored the interaction between OAM beams, ferromagnetic materials, and vortex dichroism in the AOS process Even while research into OAM-induced AOS is still in its early stages, our original proposition suggested that the OAM handedness and the

order of the topological charge, **L**, might play a deterministic role. We conclude that there is no measurable effect of either the sign or the magnitude of OAM **L**, and hence the total angular momentum **J**, of light on the AOS of the ferromagnetic thin films. In ferromagnetic films, this effect is only dependent on the SAM of the light consistent with models based on magnetic circular dichroism. Within the sensitivity of the detection method, we observe that the SAM contribution in all-optical switching is predominant compared to the OAM one. Thus, the transient change of magnetization caused is not observed. It is worth mentioning here that further studies with non-paraxial light presents an exciting avenue to be explored. We conclude, however, that while there is no dependence of OAM on the AOS, light with OAM can be used for AOS for user-defined patterning in ferromagnetic materials. Previous demonstrations of AOS have been performed using Gaussian beams and have not examined the effects of light with OAM. The interplay between magnetic structures and light with OAM can help develop spectroscopy and provide a deeper understanding of AOS's basic mechanisms.

[1] A. Kirilyuk, A. V. Kimel, and T. Rasing, Ultrafast optical manipulation of magnetic order, Reviews of Modern Physics **82**, 2731 (2010).

[2] S. Mangin, M. Gottwald, C.-H. Lambert, D. Steil, V. Uhlíř, L. Pang, M. Hehn, S. Alebrand, M. Cinchetti, G. Malinowski, Y. Fainman, M. Aeschlimann, and E. E. Fullerton, Engineered materials for all-optical helicity-dependent magnetic switching, Nature Materials **13**, 286 (2014).

[3] A. V. Kimel and M. Li, Writing magnetic memory with ultrashort light pulses, Nature Reviews Materials **4**, 189 (2019).

[4] See Supplemental Material [url], which includes Refs [26–46].

[5] M. S. El Hadri, P. Pirro, C.-H. Lambert, S. Petit-Watelot, Y. Quessab, M. Hehn, F. Montaigne, G. Malinowski, and S. Mangin, Two types of all-optical magnetization switching mechanisms using femtosecond laser pulses, Physical Review B **94**, 064412 (2016).

[6] M. S. El Hadri, M. Hehn, P. Pirro, C.-H. Lambert, G. Malinowski, E. E. Fullerton, and S. Mangin, Domain size criterion for the observation of all-optical helicity-dependent switching in magnetic thin films, Physical Review B **94**, 064419 (2016).

[7] G. Kichin, M. Hehn, J. Gorchon, G. Malinowski, J. Hohlfeld, and S. Mangin, From Multiple- to Single-Pulse All-Optical Helicity-Dependent Switching in Ferromagnetic Co / Pt Multilayers, Physical Review Applied **12**, 024019 (2019).

[8] Y. Quessab, R. Medapalli, M. S. El Hadri, M. Hehn, G. Malinowski, E. E. Fullerton, and S. Mangin, Helicity-dependent all-optical domain wall motion in ferromagnetic thin films, Physical Review B **97**, 054419 (2018).

[9] M. W. Khalid, J. Ha, M. S. E. Hadri, L. Hsu, S. Hemayat, Y. Xiao, A. Sergienko, E. E. Fullerton, and A. Ndao, Meta-Magnetic All-Optical Helicity Dependent Switching of Ferromagnetic Thin Films, Advanced Optical Materials , 2301599 (2023).

[10] C. D. Stanciu, A. V. Kimel, F. Hansteen, A. Tsukamoto, A. Itoh, A. Kirilyuk, and T. Rasing, Ultrafast spin dynamics across compensation points in ferrimagnetic GdFeCo: The role of angular momentum compensation, Physical Review B **73**, 220402 (2006).

[11] R. Medapalli, D. Afanasiev, D. K. Kim, Y. Quessab, S. Manna, S. A. Montoya, A. Kirilyuk, T. Rasing, A. V. Kimel, and E. E. Fullerton, Multiscale dynamics of helicity-dependent all-optical magnetization reversal in ferromagnetic Co/Pt multilayers, Physical Review B **96**, 224421 (2017).

[12] M. W. Khalid, J. Ha, S. Hemayat, M. S. El Hadri, E. E. Fullerton, and A. Ndao, All-Optical Magnetization Reversal in Arbitrary Geometries using Metasurfaces, in *CLEO* (2023) p. STh5C.4.

[13] K. Vahaplar, A. M. Kalashnikova, A. V. Kimel, S. Gerlach, D. Hinzke, U. Nowak, R. Chantrell, A. Tsukamoto, A. Itoh, A. Kirilyuk, and T. Rasing, All-optical magnetization reversal by circularly polarized laser pulses: Experiment and multiscale modeling, Physical Review B **85**, 104402 (2012).

[14] E. Beaurepaire, J. Merle, A. Daunois, and J. Bigot, Ultrafast Spin Dynamics in Ferromagnetic Nickel, Physical Review Letters **76**, 4250 (1996).

[15] G. Malinowski, F. Dalla Longa, J. H. H. Rietjens, P. V. Paluskar, R. Huijink, H. J. M. Swagten, and B. Koopmans, Control of speed and efficiency of ultrafast demagnetization by direct transfer of spin angular momentum, Nature Physics **4**, 855 (2008).

[16] Y. Takahashi, R. Medapalli, S. Kasai, J. Wang, K. Ishioka, S. Wee, O. Hellwig, K. Hono, and E. Fullerton, Accumulative Magnetic Switching of Ultrahigh-Density Recording Media by Circularly Polarized Light, Physical Review Applied **6**, 054004 (2016).

[17] C.-H. Lambert, S. Mangin, B. S. D. C. S. Varaprasad, Y. K. Takahashi, M. Hehn, M. Cinchetti, G. Malinowski, K. Hono, Y. Fainman, M. Aeschlimann, and E. E. Fullerton, All-optical control of ferromagnetic thin films and nanostructures, Science **345**, 1337 (2014).

[18] M. W. Khalid, J. Ha, S. Hemayat, M. S. El Hadri, E. E. Fullerton, and A. Ndao, Integration of Ultrafast Magnetism and Metasurfaces for All-Optical Helicity-Dependent Switching, in *Optica Imaging Congress* (2023) p. FTh1B.2.

[19] A. A. Sirenko, P. Marsik, C. Bernhard, T. N. Stanislavchuk, V. Kiryukhin, and S.-W. Cheong, Terahertz Vortex Beam as a Spectroscopic Probe of Magnetic Excitations, Physical Review Letters **122**, 237401 (2019).

[20] E. Prinz, M. Hartelt, G. Spektor, M. Orenstein, and M. Aeschlimann, Orbital Angular Momentum in Nanoplasmonic Vortices, ACS Photonics **10**, 340 (2023).

[21] T. D. Cornelissen, R. Córdoba, and B. Koopmans, Microscopic model for all optical switching in ferromagnets, Applied Physics Letters **108**, 142405 (2016).

[22] C. Rosales-Guzmán and A. Forbes, *How to Shape Light with Spatial Light Modulators* (SPIE PRESS, 2017).

[23] K. A. Forbes and D. L. Andrews, Orbital angular momentum of twisted light: chirality and optical activity, Journal of Physics: Photonics **3**, 022007 (2021).

[24] D. Andrews, L. Romero, and M. Babiker, On optical vortex interactions with chiral matter, Optics Communications **237**, 133 (2004).

[25] W. Löffler, D. J. Broer, and J. P. Woerdman, Circular dichroism of cholesteric polymers and the orbital angular momentum of light, Physical Review A **83**, 065801 (2011).

[26] J. H. Poynting, The wave motion of a revolving shaft, and a suggestion as to the angular momentum in a beam of circularly polarised light, Proceedings of the Royal Society of London. Series A, Containing Papers of a Mathematical and Physical Character **82**, 560 (1909).

[27] L. Allen, M. W. Beijersbergen, R. J. C. Spreeuw, and J. P. Woerdman, Orbital angular momentum of light and the transformation of Laguerre-Gaussian laser modes, Physical Review A **45**, 8185 (1992).

[28] A. M. Shaltout, V. M. Shalaev, and M. L. Brongersma, Spatiotemporal light control with active metasurfaces, Science **364**, eaat3100 (2019).

[29] A. Forbes, A. Dudley, and M. McLaren, Creation and detection of optical modes with spatial light modulators, Advances in Optics and Photonics **8**, 200 (2016).

[30] L. Marrucci, C. Manzo, and D. Paparo, Optical Spin-to-Orbital Angular Momentum Conversion in Inhomogeneous Anisotropic Media, Physical Review Letters **96**, 163905 (2006).

[31] N. Yu and F. Capasso, Flat optics with designer metasurfaces, Nature Materials **13**, 139 (2014).

[32] N. Yu, F. Aieta, P. Genevet, M. A. Kats, Z. Gaburro, and F. Capasso, A Broadband, Background-Free Quarter-Wave Plate Based on Plasmonic Metasurfaces, Nano Letters **12**, 6328 (2012).

[33] A. E. Willner, H. Huang, Y. Yan, Y. Ren, N. Ahmed, G. Xie, C. Bao, L. Li, Y. Cao, Z. Zhao, J. Wang, M. P. J. Lavery, M. Tur, S. Ramachandran, A. F. Molisch, N. Ashrafi, and S. Ashrafi, Optical communications using orbital angular momentum beams, Advances in Optics and Photonics **7**, 66 (2015).

[34] Z. Ma, M. W. Khalid, and S. Ramachandran, Long-distance Pulse Propagation of 50 Uncoupled Fiber Modes due to Topological Confinement, in *Conference on Lasers and Electro-Optics* (Optica Publishing Group, San Jose, California, 2022) p. STu4P.3.

[35] X. Zhuang, Unraveling DNA Condensation with Optical Tweezers, Science **305**, 188 (2004).

[36] D. G. Grier, A revolution in optical manipulation, Nature **424**, 810 (2003).

[37] J. Vieira, R. M. G. M. Trines, E. P. Alves, R. A. Fonseca, J. T. Mendonça, R. Bingham, P. Norreys, and L. O. Silva, Amplification and generation of ultra-intense twisted laser pulses via stimulated Raman scattering, Nature Communications **7**, 10371 (2016).

[38] F. Kong, C. Zhang, F. Bouchard, Z. Li, G. G. Brown, D. H. Ko, T. J. Hammond, L. Arissian, R. W. Boyd, E. Karimi, and P. B. Corkum, Controlling the orbital angular momentum of high harmonic vortices, Nature Communications **8**, 14970 (2017).

[39] M. Erhard, R. Fickler, M. Krenn, and A. Zeilinger, Twisted photons: new quantum perspectives in high dimensions, Light: Science & Applications **7**, 17146 (2017).

[40] T. Stav, A. Faerman, E. Maguid, D. Oren, V. Kleiner, E. Hasman, and M. Segev, Quantum entanglement of the spin and orbital angular momentum of photons using metamaterials, Science **361**, 1101 (2018).

[41] K. Y. Bliokh, F. J. Rodríguez-Fortuño, F. Nori, and A. V. Zayats, Spin–orbit interactions of light, Nature Photonics **9**, 796 (2015).

[42] K. Y. Bliokh, E. A. Ostrovskaya, M. A. Alonso, O. G. Rodríguez-Herrera, D. Lara, and C. Dainty, Spin-to-orbital angular momentum conversion in focusing, scattering, and imaging

systems, Optics Express **19**, 26132 (2011).

[43] K. Y. Bliokh, M. A. Alonso, E. A. Ostrovskaya, and A. Aiello, Angular momenta and spin-orbit interaction of nonparaxial light in free space, Physical Review A **82**, 063825 (2010).

[44] Y. Zhao, J. S. Edgar, G. D. M. Jeffries, D. McGloin, and D. T. Chiu, Spin-to-Orbital Angular Momentum Conversion in a Strongly Focused Optical Beam, Physical Review Letters **99**, 073901 (2007).

[45] Y. Hu, Z. Wang, X. Wang, S. Ji, C. Zhang, J. Li, W. Zhu, D. Wu, and J. Chu, Efficient full-path optical calculation of scalar and vector diffraction using the Bluestein method, Light: Science & Applications **9**, 119 (2020).

[46] A. M. Yao and M. J. Padgett, Orbital angular momentum: origins, behavior and applications, Advances in Optics and Photonics **3**, 161 (2011).